

Density Profiles, Casimir Amplitudes and Critical Exponents in the Two Dimensional Potts Model: A Density Matrix Renormalization Study

Enrico Carlon

Institute for Theoretical Physics, Katholieke Universiteit Leuven, Celestijnenlaan 200D, B-3001 Leuven, Belgium

Ferenc Iglói

Research Institute for Solid State Physics, H-1525 Budapest, P.O.Box 49, Hungary

Institute for Theoretical Physics, Szeged University, H-6720 Szeged, Hungary

(Preprint KUL-TF-97/25)

We use the density matrix renormalization group (DMRG) to perform a detailed study of the critical properties of the two dimensional Q state Potts model, including the magnetization and energy-density profiles, bulk and surface critical exponents and the Casimir amplitudes. We apply symmetry breaking boundary conditions to a $L \times \infty$ strip and diagonalize the corresponding transfer matrix for a series of moderately large systems ($L \leq 64$) by the DMRG method. The numerically very accurate finite lattice results are then extrapolated by efficient sequence extrapolation techniques. The critical density profiles and the Casimir amplitudes are found to follow precisely the conformal predictions for $Q = 2$ and 3. Similarly, the bulk and surface critical exponents of the models are in very good agreement with the conformal and exact values: their accuracy has reached or even exceeded the accuracy of other available numerical methods. For the $Q = 4$ model both the profiles and the critical exponents show strong logarithmic corrections, which are also studied.

PACS numbers: 05.50.+q, 05.70.J, 64.60.F, 68.35.Rh

I. INTRODUCTION

The density matrix renormalization group (DMRG) method by White¹ has considerably enhanced our abilities to diagonalize numerically the Hamiltonians of one-dimensional quantum systems. Among the systems treated so far by the DMRG method we mention Heisenberg spin chains², Heisenberg ladders³ and strongly correlated electron systems⁴. Recently, the first steps have been made towards the generalization of the method to other directions, such as two dimensional (2d) quantum systems⁵, non-Hermitian Hamiltonians⁶, etc.

According to numerical observations the DMRG method has a fast convergence, if the ground state and the excited states of the Hamiltonian are well separated, especially when the ground state wave function can be approximated as a product of tensors⁷. This happens, among others, at the valence bond solid point of the generalized antiferromagnetic $S = 1$ Heisenberg chain^{7,8}. On the other hand the convergence of the method becomes slower at the critical region. The origin of this slowing down is two-fold. First, the spectrum of the density matrix at the critical point becomes more dense and therefore more states have to be kept to guarantee a given accuracy. Second, the ground state of the Hamiltonian is nearly degenerate in the critical region and therefore the computational time needed to perform the Lánczos diagonalization increases considerably.

In the first application of the DMRG to the critical region⁹ the couplings of the Hamiltonian were subject of a renormalization procedure and the critical exponents, obtained from the fixed-point transformation, were less

accurate than those obtained by the standard renormalization group. Later studies, concentrated on two dimensional classical systems^{10–12}, have demonstrated that the thermodynamic properties of the critical systems can be accurately obtained by the DMRG method. In a 2d classical system it is natural to consider the row-to-row transfer matrix and calculate its leading eigenvalues by the DMRG method, as done first by Nishino¹⁰. More recently, the DMRG method and Baxter's corner transfer matrix¹³ have been combined in an efficient iterative algorithm¹⁴.

In this article we use the DMRG method to study the critical properties of the two dimensional Q state Potts model, in particular we focus on the behavior of local densities, as the magnetization and the energy density, and on the Casimir amplitudes for $L \times \infty$ strips with symmetry breaking boundary conditions. These quantities have been derived from conformal invariance, but to our knowledge, never computed directly from a lattice calculation. We also calculate the complete set of surface and bulk critical exponents and compare our results with the exact ($Q = 2$) and conjectured values ($Q = 3, 4$) for these exponents.

In the usual DMRG procedure the thermodynamic limit is approached by simply increasing the size of the system; typically one considers quantum chains of lengths of the order of 10^3 , which are generated by many DMRG iterations. Quantities as order parameters and correlation lengths are calculated from such large lattices. The drawback of this approach is that for such large systems the accuracy of the DMRG method is not as good as for chains of length of one order of magnitude smaller, especially at the critical point, for the reasons discussed

above. On the other hand in the traditional finite size scaling analysis¹⁵, which is based on a numerically exact diagonalization of the Hamiltonian by the Lánczos method, the size of the finite lattices are of the order of 10, which is often too small value for an accurate determination of critical exponents from finite size scaling.

In the present study we combine the standard finite size scaling analysis with the computational power of the DMRG method. Using White's finite system algorithm¹⁶ we calculate quantities with very high accuracy for strips of moderate widths ($L \leq 64$). The advantage with respect to the exact diagonalization of small lattices is that the finite size scaling is performed on a wider range of system sizes, corrections to scaling have weaker effects and one can determine critical exponents with a high accuracy. Through the finite system DMRG algorithm one is also able to calculate accurately not only bulk, but at the same time also surface exponents, obtaining thus a deeper knowledge of the critical properties of the system.

The structure of the paper is the following. In Section II we describe the DMRG method and its application to the Q state Potts model. Our results about the critical density profiles are presented in Section III, whereas the critical exponents and the Casimir amplitudes are investigated in Section IV. Finally, in Section V we discuss our results.

II. THE DMRG METHOD AND ITS APPLICATION TO THE POTTS MODEL

The Q state Potts model¹⁷ - due to many exact and conjectured results - is an important testing ground for different approximate theories and numerical methods in statistical physics. We consider a $L \times \infty$ lattice labeled by $l = 1, 2 \dots L$ and $-\infty < k < \infty$ with an Hamiltonian written as

$$\beta H = -K \sum_k \sum_{l=1}^L \{ \delta(s_{l,k} - s_{l+1,k}) - \delta(s_{l,k} - s_{l,k+1}) \} \quad (1)$$

in terms of a Q component spin variable $s_{l,k} = 0, 1, \dots, Q-1$ (β denotes the inverse temperature). In the following we take $\beta = 1$ and consider the ferromagnetic model ($K > 0$). In this case one can obtain the phase transition point of the system

$$e^K = 1 + \sqrt{Q}, \quad (2)$$

and the energy per bond at the transition point

$$\epsilon_0 = \frac{1}{2} \left(1 + \frac{1}{\sqrt{Q}} \right). \quad (3)$$

from a duality transformation¹⁷. For general Q the model is integrable *at the transition point* and the transition is of second (first) order for $Q \leq 4$ ($Q > 4$)¹⁸. In this paper we restrict ourselves to the second order transition regime.

Since the model - except of the case of the $Q = 2$ (Ising model) - is not solved outside of the critical point the critical exponents are not known exactly for general Q . Their values, however, are conjectured by conformal field theory^{19–21} and by approximate mappings²².

In a $L \times \infty$ strip the local densities, such as the magnetization

$$m_L(l) = \frac{Q \langle \delta(s_{l,k}) \rangle - 1}{Q - 1}, \quad (4)$$

and the singular part of the energy density

$$\epsilon_L(l) = \langle \delta(s_{l,k} - s_{l+1,k}) \rangle - \epsilon_0, \quad (5)$$

depend on the position of the layers $l = 1, 2 \dots L$.

In the transfer matrix formalism the elements of the row-to-row transfer matrix T_L are labeled by the possible states of a row in the system: $i = 1, 2, \dots, Q^L$. The leading eigenvalue λ_L of the transfer matrix

$$T_L |v_L\rangle = \lambda_L |v_L\rangle, \quad (6)$$

gives the free energy per spin as

$$f_L = -\frac{1}{L} \ln \lambda_L. \quad (7)$$

If the dominant eigenvector $|v_L\rangle$ is normalized, the squares of its elements $v_L^2(i)$ are equal to the probabilities of finding a row in a state i . Average quantities as $\langle \delta(s_{l,k}) \rangle$ can be calculated then:

$$\langle \delta(s_{l,k}) \rangle = \sum_{i=1}^{Q^L} v_L^2(i) \delta(s_l(i)), \quad (8)$$

where $s_l(i)$ denotes the value of the l -th spin for a row in the i -th configuration. In this way one derives magnetization and energy density profiles from the dominant eigenvector $|v_L\rangle$.

The problem of the transfer matrix approach is that a numerically exact solution of the eigenvalue equation (6) is restricted to small lattices, since the dimensionality of the spin space grows rapidly with the strip width L . Finite size results derived from transfer matrix calculations can be extrapolated only for a limited range of values of L .

The DMRG provides a very efficient algorithm for the construction of effective transfer matrices \tilde{T}_L of large $L \times \infty$ strips, which are generated iteratively from a transfer matrix of a strip of a small width (L_0) which can be diagonalized exactly. In the initial step a row of the $L_0 \times \infty$ strip is divided into two parts A and B , which are labeled by variables $1 \leq j_A \leq N_A$ and $1 \leq j_B \leq N_B$, such that $i \equiv (j_A, j_B)$ and $N_A N_B = Q^{L_0}$. Typically we split the system into two subsystems of the same size, i.e. $N_A = N_B$, although this is not strictly necessary.

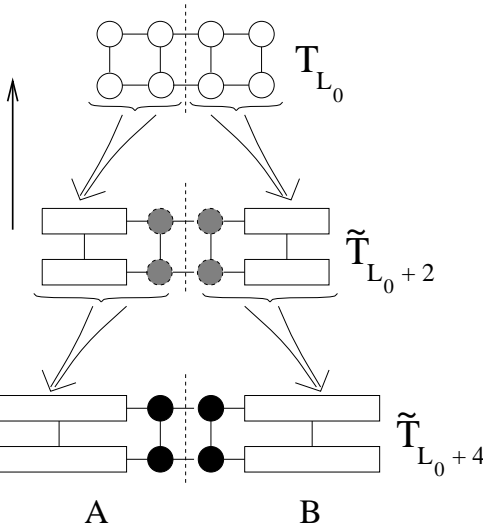


FIG. 1. Schematic view of the DMRG algorithm for the construction of effective transfer matrices \tilde{T}_L (the arrow denotes the transfer direction). Starting from a small system ($L_0 = 4$ in the example) the strip width is enlarged by two spins at each iteration. New spins are added at the center of the strip and rectangles denote blocks containing several spins, but labeled by m states only.

In the construction of a larger strip only part of the states of the A and B subsystems are kept, namely the eigenstates of the density matrices of A and B corresponding to the largest eigenvalues. The elements of the density matrix for the subsystem A are defined as follows:

$$\rho^{(A)}(l_A, k_A) = \sum_{j_B=1}^{N_B} v_{L_0}(l_A, j_B) v_{L_0}(k_A, j_B) \quad (9)$$

where the sum is extended to all possible states of the subsystem B . The density matrix eigenvalues ω_r , which we order according to $\omega_1 > \omega_2 > \dots > \omega_{N_A}$, are equal to the probabilities of finding the subsystem A in the corresponding eigenvectors $|\Omega_r\rangle$ when the whole system is in a state $|v_{L_0}\rangle$. In the calculation the spin space of the subsystem A is truncated and one keeps m eigenvectors $|\Omega_r\rangle$ corresponding to the largest eigenvalues. The truncation error, defined as:

$$\epsilon = 1 - \sum_{r=1}^m \omega_r \quad (10)$$

gives an estimate of the accuracy of the procedure. For $m = N_A$ (all states kept) obviously $\epsilon = 0$; typically the density matrix eigenvalues ω_r decrease rapidly with the index r , so good accuracy can be reached with a moderate number of states kept. The truncated subsystem A is enlarged by adding an extra Potts spin; the old subsystem plus the spin corresponds to a new subsystem A , labeled now by mQ states. An analogous procedure is followed for the subsystem B , whose spin space is first truncated by the selection of the dominant m eigenvalues of the density matrix for the B part $\rho^{(B)}$, and then

enlarged by an extra spin. Combining the two new subsystems A and B together one obtains a transfer matrix \tilde{T}_{L_0+2} for a $(L_0+2) \times \infty$ strip. The procedure is repeated until the strip of the wanted width has been generated:

$$T_{L_0} \rightarrow \tilde{T}_{L_0+2} \rightarrow \tilde{T}_{L_0+4} \rightarrow \dots \rightarrow \tilde{T}_L. \quad (11)$$

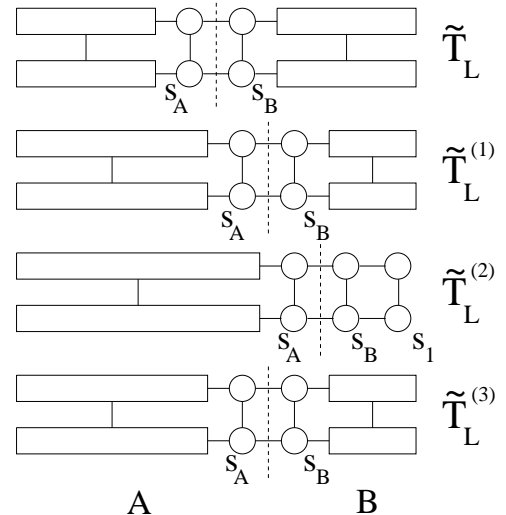


FIG. 2. Schematic view of White's finite system method. Only one of the two subsystems grows at each iteration: subsystem A in the first two iterations and subsystem B in the third. The spins s_A and s_B sweep through the strip width; from the transfer matrix $\tilde{T}_L^{(2)}$ one calculates, for instance, the average magnetization of the surface spin s_1 .

A schematic view of the first iterations is shown in Fig. 1. In each DMRG step one solves the eigenvalue equation:

$$\tilde{T}_L |\tilde{v}_L\rangle = \tilde{\lambda}_L |\tilde{v}_L\rangle \quad (12)$$

defined in a $Q^2 m^2 \times Q^2 m^2$ space. The quantity $\tilde{f}_L = -\ln(\tilde{\lambda}_L)/L$ approximate the exact free energy f_L of the $L \times \infty$ strip and from the dominant eigenvector $|\tilde{v}_L\rangle$ one can calculate the magnetizations of the spins $s_{L/2,k}$ and $s_{L/2+1,k}$ at the center of the strip (see Fig. 1) and the energy density of the bond connecting them.

The iterations in (11) describe White's infinite system algorithm¹⁶. Repeating the procedure many times one generates transfer matrices of very large systems: at each iterations new spins are added at the center of the strip and the boundaries are pushed farther away from each other (see Fig. 1). Notice also that we implement open boundary conditions, as commonly done for DMRG calculations since it has been found that the accuracy is the best in this case¹⁶.

For the calculation of the whole profile one must perform more DMRG iterations keeping the system size fixed:

$$\tilde{T}_L \rightarrow \tilde{T}_L^{(1)} \rightarrow \tilde{T}_L^{(2)} \rightarrow \dots \rightarrow \tilde{T}_L^{(q)}, \quad (13)$$

as shown schematically in Fig. 2 (we have taken $q \approx 4L$ in our calculations). In each of the iterations of (13) a spin is added only to one of the two subsystems, say to A , following the scheme described above. For the part B one takes smaller subsystems generated in the previous DMRG iterations. This procedure is continued until the subsystem B contains $L_0/2$ spins only, i.e. is known exactly. Then in each of the following steps a spin is added to B until the subsystem A contains $L_0/2$ only. In the present calculation this procedure has been repeated a couple of times.

In the iterations (13) the two spins s_A and s_B of Fig. 1 sweep through the whole strip width and from the sequence $|\tilde{v}_L\rangle, |\tilde{v}_L^{(1)}\rangle, |\tilde{v}_L^{(2)}\rangle, \dots$ one calculates the magnetization and energy density profiles across the strip. At the same time the free energies calculated from the eigenvalues of the transfer matrices $\tilde{T}_L^{(i)}$ of (13) decrease at each iteration $\tilde{f}_L^{(i)} \leq \tilde{f}_L^{(i+1)}$ getting closer and closer to the exact free energy f_L (it is known⁷ that DMRG free energies provide upper bounds for f_L).

The steps in (13) describe the so-called finite system algorithm¹⁶, which is particularly indicated for the study of finite systems, since it provides higher accuracy than the infinite system method. The procedure is more time consuming, but has the advantage of providing information about the whole strip and it is necessary to calculate density profiles¹¹.

Using the finite system method we have generated effective transfer matrices for strips of widths $L = 8, 16, 24, \dots, 64$ at the system critical point. We have used $m = 32$ for $Q = 2$, $m = 60$ for $Q = 3$ and $m = 80$ for $Q = 4$; in each cases the truncation error was $\epsilon < 10^{-10}$. It is not possible to relate the value of ϵ with the actual errors for the free energy and the density profiles. On the basis of our experience we expect an accuracy of 8–9 digits for the density profiles for $L \leq 64$ and a somewhat higher accuracy for the free energy.

III. CRITICAL DENSITY PROFILES

In a critical system confined between two parallel plates, being a large but finite distance L apart, the local densities $\langle \Phi(r) \rangle$ such as the magnetization and the energy density vary with the distance l as a smooth function of l/L . According to the scaling theory by Fisher and de Gennes²³

$$\langle \Phi(l) \rangle_{ab} = l^{-x_\Phi} F_{ab}(l/L), \quad (14)$$

where ab denotes the boundary conditions (b.c.) applied at the two plates and x_Φ is the scaling dimension of the operator Φ . For the magnetization and the energy density operators their value are connected with the more common critical exponents as:

$$x_m = \beta/\nu \quad \text{and} \quad x_\epsilon = d - 1/\nu = (1 - \alpha)/\nu \quad (15)$$

where β , ν and α are the magnetization, correlation length and specific heat critical exponents, respectively, while d denotes the dimensionality of the system.

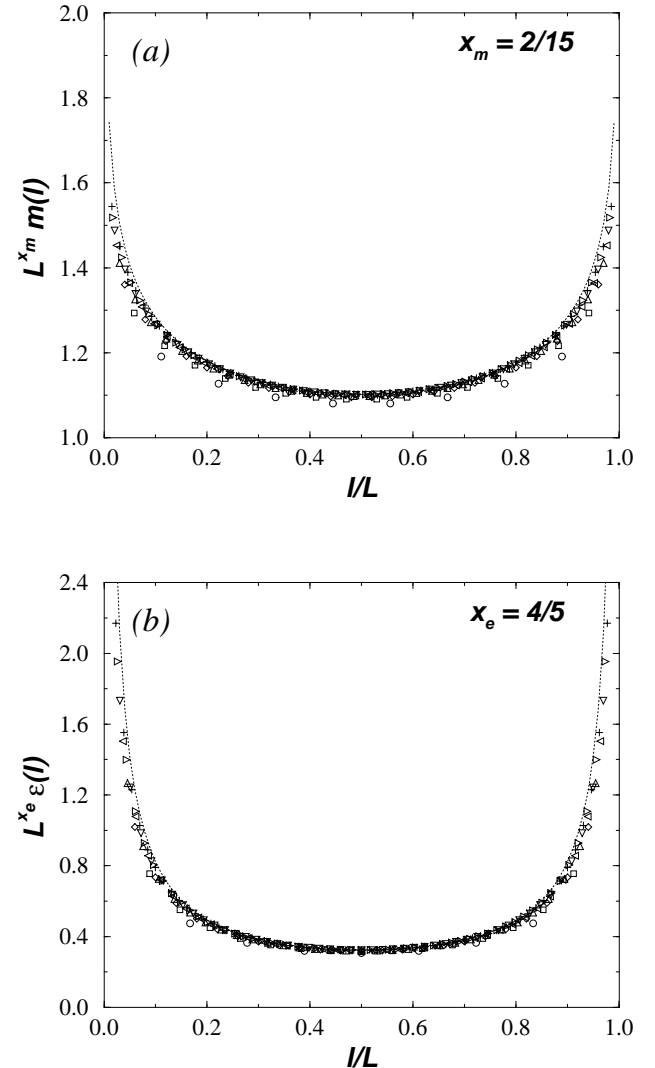


FIG. 3. Scaled magnetization (a) and energy density (b) profiles for the $Q = 3$ Potts model with fixed and equal spins at the boundaries. The symbols corresponds to $L \times \infty$ strips with $L = 8$ (circles), $L = 16$ (squares), $L = 24$ (diamonds), $L = 32$ (triangles up), $L = 40$ (triangles down), $L = 48$ (triangles left), $L = 56$ (triangles right) and $L = 64$ (pluses). The dotted lines are the conformal invariance predictions for the profiles. Also the values of the critical indices x_m and x_e used for the scaled profiles are indicated.

The scaling function F_{ab} in Eq. (14) has the following asymptotic behavior:

$$F_{ab}(l/L) = \mathcal{A} \left[1 + B_{ab} \left(\frac{l}{L} \right)^d + \dots \right] \quad \frac{l}{L} \ll 1, \quad (16)$$

where B_{ab} , the Fisher-de Gennes coefficients are connected to universal quantities.

In two dimensions conformal invariance predicts the following form for the critical profiles with general conformally invariant b.c.^{25,24}:

$$\langle \Phi(l) \rangle_{ab} = \left[\frac{L}{\pi} \sin \left(\frac{\pi l}{L} \right) \right]^{-x_\phi} G_{ab} \left[\cos \left(\frac{\pi l}{L} \right) \right], \quad (17)$$

where the scaling function $G_{ab}(\omega)$ depends on the universality class of the model and on the type of b.c. applied. Expanding Eq. (17) for $l/L \ll 1$ one finds that the Fisher-de Gennes coefficients B_{ab} in Eq. (16) are given by:

$$B_{ab} = \pi^2 \left[\frac{x_\Phi}{6} - \frac{1}{2} \frac{G_{ab}'(1)}{G_{ab}(1)} \right]. \quad (18)$$

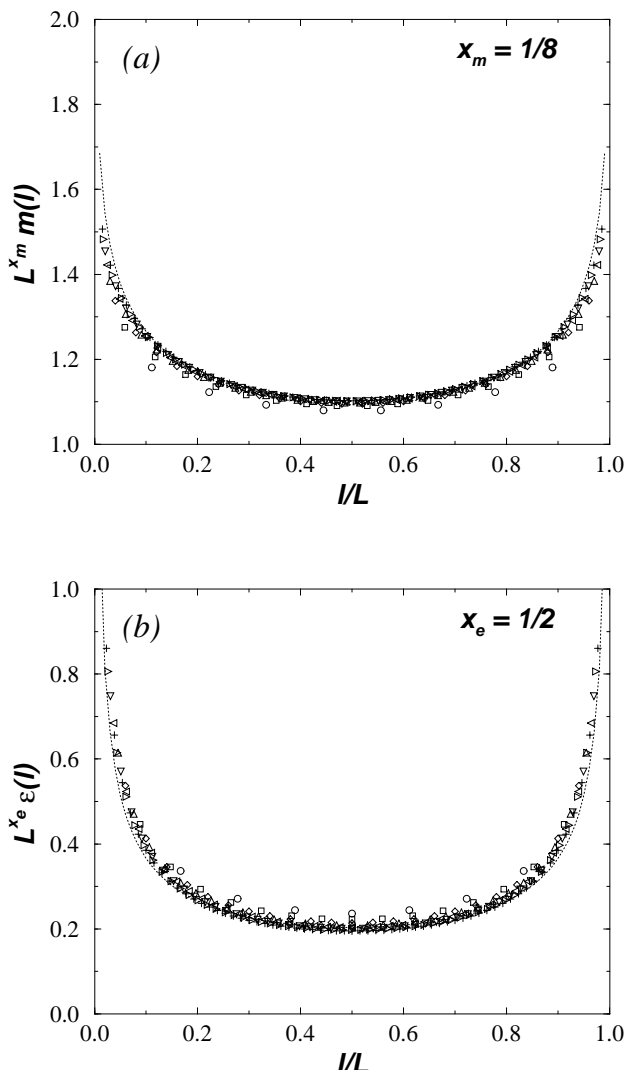


FIG. 4. As in Fig. 3, but for $Q = 4$.

In this section we present the critical profiles for the magnetization and the energy density calculated with the DMRG method and compare them with the predictions of conformal invariance (17). We have performed the calculations for $Q = 2, 3$ and 4 with all types of conformally invariant b.c. Here - for the sake of brevity - we present only the results for $Q = 3$ and 4 . The $Q = 2$ (Ising) results, which can be calculated more efficiently by the Pfaffian technique²⁶, will be used in the next Section to calculate the critical exponents of the model. For all b.c. used we found that the $Q = 2$ magnetization and energy density profiles agree well with the conformal results of Eq. (17).

We start with the parallel spin b.c., i.e. we fix spins to the same state $s = 0$ at the two boundaries and we indicate this choice by setting $a = b = 0$ in Eq. (17). According to conformal invariance²⁷ the scaling function in Eq. (17) both for the magnetization and the energy density is a constant: $G_{00} = \text{const.}$ Notice that Eqs. (14) and (17) imply that the scaled density profile $L^{x_\phi} \langle \phi(l) \rangle_{ab}$ depends on l only through the variable l/L . In Figs. 3 and 4 we show the scaled magnetization and energy density profiles for the $Q = 3$ and $Q = 4$ models, respectively, together with the conformal results. As seen in the Figures the DMRG data corresponding to different values of L collapse into single scaling curves, which are in good agreement with the conformal results. In the scaling plot we have used the values of the scaling dimensions conjectured by conformal field theory and which are given in Table III. These scaling dimensions will be computed from a finite size scaling analysis of the DMRG data in the next Section. Notice that the magnetization profiles of Fig. 3(a) and Fig. 4(a) differ only slightly since the magnetic exponents in the $Q = 3$ and $Q = 4$ Potts model are very close to each other. A more visible difference between the $Q = 3$ and the $Q = 4$ case can be seen in the energy density profiles of Figs. 3(b) and 4(b).

As next case we consider the fixed-free b.c., i.e. we fix the spins to the state $s = 0$ only at one boundary of the system; we indicate these b.c. by setting $a = 0, b = f$ in Eq. (17). The scaling behavior of the critical densities in a free surface are governed by the surface scaling dimensions²⁸, which are generally different from the corresponding bulk quantities. For the Q state Potts model the surface magnetization scaling dimensions

$$x_m^s = \beta_s / \nu, \quad (19)$$

where β_s is the surface magnetization critical exponent, are listed in Table III as derived by conformal field theory²¹. We recall that the value of the surface energy scaling dimension is universally $x_e^s = 2$ for two dimensional models²⁹. The conformal prediction²⁵ about the scaling function in the critical profiles in Eq. (17) is:

$$G_{0f}^m = \mathcal{A} \left[\cos \left(\frac{\pi l}{2L} \right) \right]^{x_m^s} \quad (20)$$

for the magnetization and

$$G_{0f}^e = \mathcal{B} \cos\left(\frac{\pi l}{L}\right) \quad (21)$$

for the energy density (\mathcal{A} and \mathcal{B} are constants).

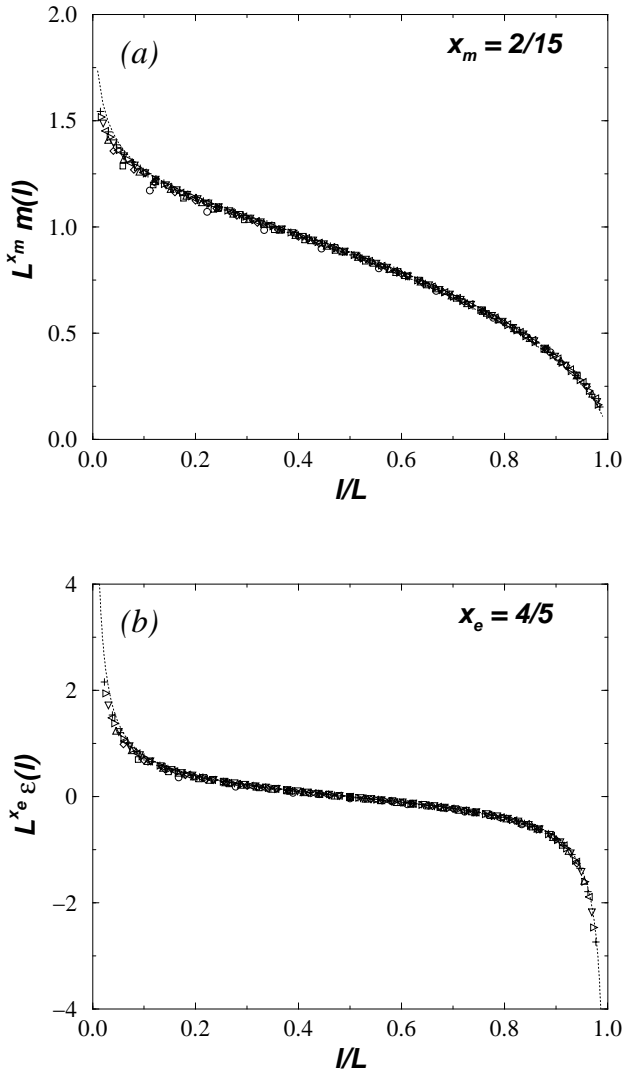


FIG. 5. Scaled magnetizations (a) and energy densities (b) for $Q = 3$ in strips with fixed free boundary conditions. The symbols are as in Fig. 3.

Figures 5 and 6 show the scaled magnetization and energy density profiles with fixed-free b.c. for $Q = 3$ and $Q = 4$, respectively. The data collapse into single scaling curves which are in good agreement with the conformal invariance predictions (20) and (21), except for the magnetization profiles of the $Q = 4$ state Potts model as shown in Fig. 6(a) where one finds strong deviation of the numerical data from the conformal invariance results. The origin of these discrepancies is the presence of very strong, logarithmic corrections to scaling in the

$Q = 4$ model³⁰. As will be discussed in the next Section the leading $1/\ln L$ corrections to finite size scaling are universal and they can be taken into account using effective, size dependent scaling dimensions. We made use the same strategy here and for the largest finite system with $L = 64$ we compared the DMRG data with the conformal results, where in Eqs. (17), (20) the corresponding effective scaling dimensions were used. As seen in the inset of Fig. 6(a) we have obtained good agreement with the corrected formula.

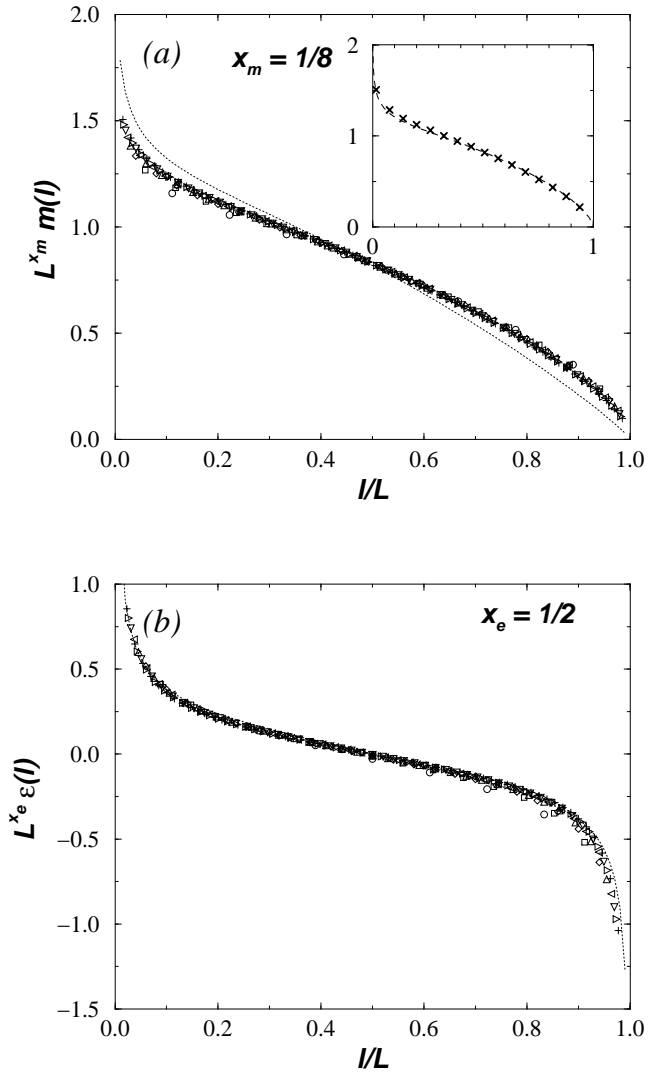


FIG. 6. As in Fig. 5 for $Q = 4$. The inset of (a) shows the DMRG data for $L = 64$ (crosses) and the conformal profile of Eq. (17), (20) where we have used effective size dependent scaling dimensions $x_m(L)$ and $x_m^s(L)$ given in (31) and (33) with $L = 64$.

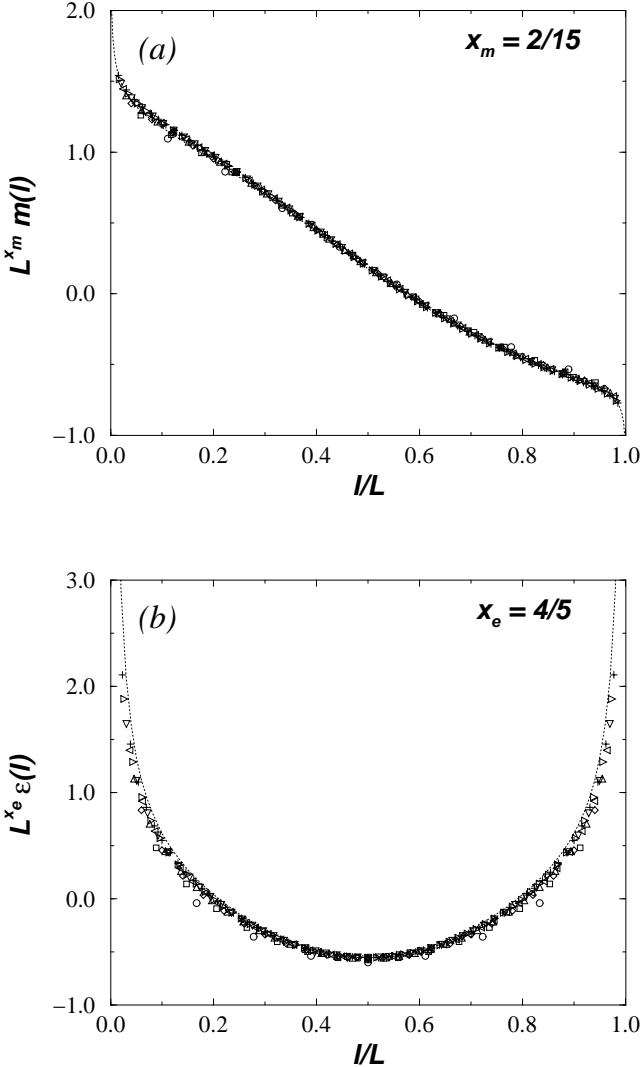


FIG. 7. Scaled magnetizations (a) and energy density profiles (b) in strip with mixed boundary conditions for $Q = 3$. The symbols are as in Fig. 3.

Finally, we consider the third type of conformally invariant b.c., when the two boundary layers are fixed to different states, say $a = 0$ and $b = 1$. The conformal predictions about the scaling functions in Eq. (17) are in this case the most complicated²⁵. For the magnetization profile the scaling function $G_{01}^m(\omega)$ is expressed by a combination of hypergeometric functions, which reduces to polynomials for $Q = 2$, where $G_{01}^m(\omega) = \mathcal{A}\omega$ and for $Q = 4$, where $G_{01}^m(\omega) = \mathcal{B}(1 + 4\omega + \omega^2)$. For the energy density profile the scaling function

$$G_{01}^e = \mathcal{C} \left[1 - 8 \frac{1 - x_e/2}{5 - 4x_e} \sin^2 \left(\frac{\pi l}{L} \right) \right] \quad (22)$$

involves the energy scaling dimension x_e (\mathcal{A} , \mathcal{B} and \mathcal{C} denote non-universal constants).

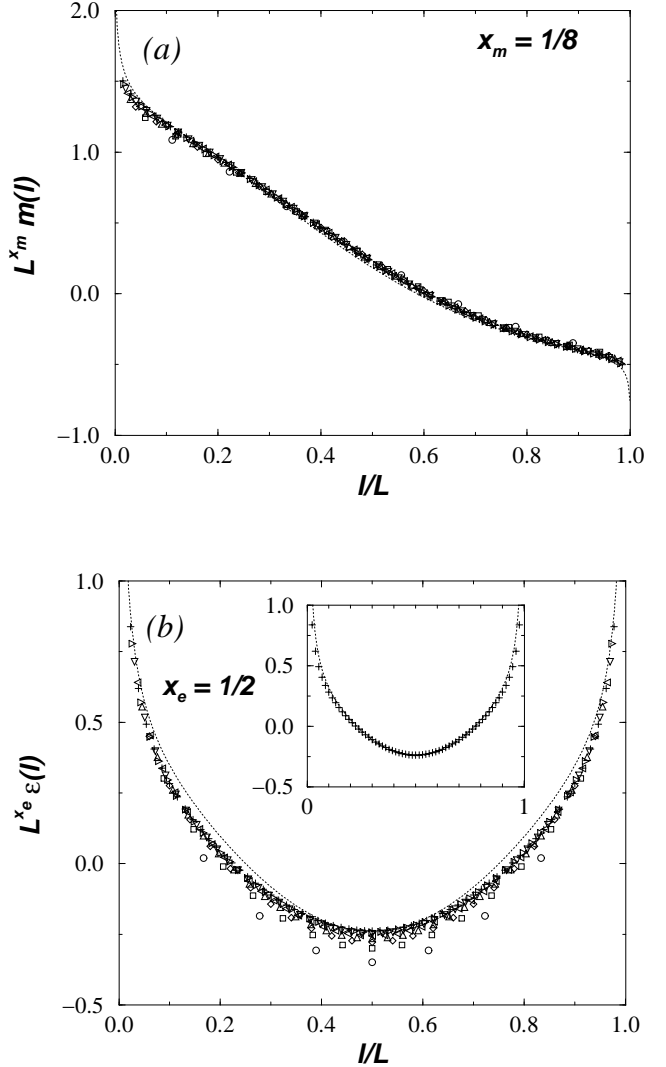


FIG. 8. As in Fig. 7 for $Q = 4$. The inset of (b) shows the DMRG data for $L = 64$ (pluses) and the profile obtained from conformal invariance where we have used an effective size dependent critical index $x_e(L)$ given in Eq. (32), for $L = 64$.

Figures 7 and 8 show the scaled magnetization and energy density profiles for $Q = 3$ and $Q = 4$ for mixed boundary conditions. In the $Q = 3$ case the numerical data referring to strips of different widths collapse into single curves which are in very good agreement with the conformal invariance predictions. For the case $Q = 4$ the agreement with conformal invariance is worse, again due to the logarithmic corrections. The strongest corrections are found for the energy density profile Fig. 8(b); the data collapse is clearly worse than in the $Q = 3$ case for the energy density. As done for the fixed-free boundary conditions we consider finite size approximants to the conformal profile (22), by substituting the exponent x_e appearing in Eq. (22) with $x_e(L)$ for $L = 64$. Also in this case the modified conformal profile with an effective size

dependent exponent agrees quite well with the numerical data as seen in the inset of Fig. 8(b).

IV. CRITICAL EXPONENTS AND CASIMIR AMPLITUDES

In this Section we perform a quantitative analysis of the finite lattice data obtained by the DMRG method. First, we consider the various critical exponents, then we investigate the finite size dependence of the free-energy density and calculate the Casimir amplitudes with different boundary conditions.

A. Critical exponents

The critical exponents such as x_m , x_e and x_m^s defined in Eqs. (15) and (19) can be calculated by two different methods. In the first method, which is more general and not restricted to two dimensional systems, we use the *scaling form* of Eq. (14). The second way of determination of the critical exponents is based on *conformal invariance*: we use explicitly the functional form of the density profiles presented in Sec. III.

We start with the scaling method and compare the values of a density, for instance the magnetization $m_L(l)$ for different widths L , which are taken as $L = 8, 16, \dots, 64$, and at constant values of $z = l/L$. The corresponding scaling dimension - x_m - is obtained as the limiting value of the finite lattice estimates:

TABLE I. Table of the BST extrapolants for the bulk magnetization exponent for the $Q = 3$ Potts model calculated from finite size scaling at the center of the strip with fixed identical spins at the boundaries. (The parameter of the BST algorithm is $\epsilon = 5/6$.)

0.108817	0.128823	0.133723	0.133518	0.133505	0.133511	0.133715
0.116774	0.131197	0.133577	0.133465	0.133510	0.133801	
0.120575	0.132097	0.133514	0.133431	0.133603		
0.122859	0.132535	0.133475	0.133409			
0.124400	0.132781	0.133449				
0.125517	0.132933					
0.126367						

For the calculation of the scaling dimension x_e we have used an expression similar to Eq. (23) with the magnetization replaced by the energy density profile. The surface exponent x_m^s follows from the analysis of the magnetization profile for fixed-free boundary conditions; according to scaling theory the magnetization of the surface spin at criticality in a $L \times \infty$ strip scales as:

$$m_L^s \sim L^{-x_m^s} \quad (25)$$

$$x_m(L) = \frac{\ln(m_L/m_{L+8})}{\ln(1+8/L)}, \quad (23)$$

which - according to scaling theory - is independent of $0 < z < 1$ (in the previous formula $m_L \equiv m_L(zL)$ and $m_{L+8} \equiv m_{L+8}[z(L+8)]$).

Following traditional finite size scaling methods¹⁵ we extrapolate the finite lattice approximants $x_m(L)$ to $L \rightarrow \infty$, using a powerful sequence extrapolation technique, such as the widely used BST-method³¹. Here, we are not going to recapitulate the details of this extrapolation procedure just for illustration we present the table of extrapolants (Table I) for x_m obtained at the middle point ($z = 1/2$) of the magnetization profiles of the $Q = 3$ Potts model with parallel-spin boundary conditions. From the original series, which is in the first column of Table I and calculated through Eq. (23), new extrapolants are generated by the repeated use of the BST algorithm, which are shown in the successive columns. One generally expects faster convergence within the data in higher order columns. As one can see in Table I there is a nice convergence up to the third and fourth column, which however is not increased in the further steps. Thus our estimate of the magnetic scaling dimension based on the BST algorithm is

$$x_m = 0.1334(1) \quad (Q = 3), \quad (24)$$

which agrees very well with the conformal result $x_m = 2/15^{19,20}$, and it is at least as accurate as the other existing numerical results³².

from which one can extract the surface exponent in an analogous way as done for x_m (see Eq. (23)).

Next, we are going to describe our second way of calculating the critical exponents, which is based on the conformal results about the profiles. As an example we consider the magnetization profile with fixed-free b.c. in Eqs. (17), (20) and take three points from the profile for a strip of given width L : $m_L(L/4)$, $m_L(L/2)$ and $m_L(3L/4)$. It is easy to see that the surface magnetiza-

tion exponent x_m^s is approximated as:

$$x_m^s(L) = \frac{\ln [m_L(\frac{L}{4})/m_L(\frac{3L}{4})]}{\ln(\sqrt{2}+1)}, \quad (26)$$

whereas the bulk exponent x_m is involved in the combi-

nation:

$$x_m(L) - \frac{x_m^s(L)}{2} = \frac{\ln [m_L(\frac{L}{4})m_L(\frac{3L}{4})/m_L(\frac{L}{2})^2]}{\ln 2}. \quad (27)$$

TABLE II. Table of the BST extrapolants for the surface magnetization exponent for the $Q = 3$ Potts model calculated from Eq. (26). (The parameter of the BST algorithm is $\epsilon = 5/6$.)

0.554998	0.673224	0.668052	0.667014	0.666865	0.666938	0.666666
0.584425	0.670860	0.667623	0.666936	0.666799	0.666574	
0.600929	0.669696	0.667388	0.666880	0.666762		
0.611585	0.669012	0.667238	0.666839			
0.619076	0.668565	0.667136				
0.624650	0.668252					
0.628972						

Using other profiles one can easily obtain relations for the bulk (magnetization or energy) exponents, as well. To illustrate the accuracy of the conformal method we show in Table II the BST extrapolants of the surface magnetization exponent, calculated from Eq. (26) for the $Q = 3$ model. Here, one can see a similar tendency in the extrapolations as in Table I for the finite size data. The obtained estimate of the surface exponent

$$x_m^s = 0.6667(1) \quad (Q = 3), \quad (28)$$

is again in excellent agreement with Cardy's conformal result $x_m^s = 2/3^{21}$. We note that our estimates on the critical exponents for a given model, obtained by the scaling and the conformal methods are consistent and the errors of the two methods are also comparable. The same is true if other type of profiles or other points of the profiles are considered. We used this freedom to obtain an objective criterion about the error of our estimates.

Our results for the critical exponents calculated by the DMRG method are presented in Table III together with

$$f(t, h, h_s, \Psi, L) = L^{-d} f(L^{2-x_e} Z^{3/4} t, L^{2-x_m} Z^{1/16} h, L^{1-x_m^s} Z^{-1} h_s, Z\Psi, 1), \quad (29)$$

with

$$Z = \left(1 - \frac{\Psi(0)}{\pi} \ln L\right)^{-1}. \quad (30)$$

Now the different physical quantities can be obtained through differentiation and then their singular behavior at the critical point can be studied by finite size scaling. It is easy to see from Eq. (29) that the critical exponents determined by this way have universal $1/\ln L$ corrections, which does not depend on $\Psi(0)$:

the exact and conformal results. The estimates are most accurate for the $Q = 2$ Ising model, which has two reasons. First, the structure of confluent singularities are the simplest for this model, and second, the numerical accuracy of the DMRG method is also the most accurate in this case. The estimates for the $Q = 3$ model are still very accurate, as a matter of fact the accuracy of the DMRG method in this case is comparable or even higher than other numerical methods (Monte Carlo simulation³³, series expansion³⁴, traditional finite size scaling³², corner transfer matrix approach^{14,35}, etc).

The $Q = 4$ state model, for which the estimates in Table III are less accurate, needs special considerations. It is known from a RG analysis that the critical Hamiltonian of the model involves a marginal scaling field Ψ , which results in logarithmic corrections to scaling. Then the finite-size scaling behavior of the free-energy density of the model as a function of the bulk (t, h) and surface (h_s) scaling fields is given by^{30,36}:

$$x_m(L) = \frac{1}{8} + \frac{1}{16} \frac{1}{\ln L} + O[(\ln L)^{-2}] \quad (31)$$

$$x_\epsilon(L) = \frac{1}{2} + \frac{3}{4} \frac{1}{\ln L} + O[(\ln L)^{-2}] \quad (32)$$

$$x_m^s(L) = 1 - \frac{1}{\ln L} + O[(\ln L)^{-2}] \quad (33)$$

Then, the appropriate strategy to analyze the finite size estimates for the exponents³⁷, such as for the bulk

magnetization scaling dimension x_m , is to consider the series of effective exponents $x_m(L) - 1/(16 \ln L)$, which has then only $(1/\ln L)^2$ corrections. The results of this type of analysis are presented in Table III, which are

TABLE III. Comparison between exact (\dagger) or conjectured (\ddagger) bulk and surface exponents for the $Q \leq 4$ Potts model and the numerical results obtained from finite size scaling extrapolations of DMRG data.

Q	x_m	x_m (DMRG)	x_{m_s}	x_{m_s} (DMRG)	x_ϵ	x_ϵ (DMRG)
2	$1/8^\dagger$	0.125000(2)	$1/2^\dagger$	0.500000(5)	1^\dagger	1.00000(1)
3	$2/15^\ddagger$	0.1334(1)	$2/3^\ddagger$	0.6667(1)	$4/5^\dagger$	0.800(1)
4	$1/8^\ddagger$	0.120(5)	1^\ddagger	1.02(2)	$1/2^\dagger$	0.49(2)

TABLE IV. Comparison of Casimir amplitude predicted by conformal invariance (CI) and the numerical values obtained from extrapolations of the numerical data (DMRG) for different types of boundary conditions.

	Q=2	Q=3	Q=4
A_{00} (CI)	$-0.0654498 \left(-\frac{\pi}{48}\right)$	$-0.10472 \left(-\frac{\pi}{30}\right)$	$-0.1309 \left(-\frac{\pi}{24}\right)$
A_{00} (DMRG)	-0.065447(5)	-0.104(1)	-0.127(5)
A_{0f} (CI)	$0.13089969 \left(\frac{\pi}{24}\right)$	$0.287979 \left(\frac{11\pi}{120}\right)$	$0.6545 \left(\frac{5\pi}{24}\right)$
A_{0f} (DMRG)	0.1309003(5)	0.2865(10)	0.67(3)
A_{01} (CI)	$1.5053465 \left(\frac{23\pi}{48}\right)$	$1.989675 \left(\frac{19\pi}{30}\right)$	$3.0107 \left(\frac{23\pi}{24}\right)$
A_{01} (DMRG)	1.505350(5)	1.987(5)	2.93(10)

B. Casimir Amplitudes

In the strip geometry with general conformally invariant boundary conditions the finite size dependence of the critical free energy-density is given as:

$$f_{ab}(L) = f_0 + \frac{f_a + f_b}{L} + \frac{A_{ab}}{L^2} + \dots, \quad (34)$$

where the bulk - f_0 - and the surface - $f_a + f_b$ - contributions are non-universal. The second-order correction term A_{ab} , known as Casimir amplitude, involves universal quantities. As shown in Refs.^{24,25}, the Casimir amplitude and the Fisher-de Gennes parameter B_{ab} in Eq. (16) are related as

$$A_{ab} = -\frac{c}{4\pi x_\Phi} B_{ab}^\Phi, \quad (35)$$

where c denotes the conformal anomaly number or central charge. We recall that $c = 1/2$ for $Q = 2$, $c = 4/5$ for $Q = 3$ and $c = 1$ for $Q = 4$. From Eq. (35) combined with the results about the profiles in Section III one obtains the values of the Casimir amplitudes predicted by

in satisfactory agreement with the conformal results and also give support to the validity of the RG analysis leading to Eq. (29).

conformal invariance. The simplest case is that of equal spins at the boundary for which the Casimir amplitude is just proportional to the conformal anomaly:

$$A_{00} = -\frac{\pi}{24} c. \quad (36)$$

In the numerical calculation we made use of Baxter's exact result about the bulk free energy-density¹⁸ for the Q state Potts model which is given by the following formula:

$$f_0 = \frac{\ln Q}{2} + \int_{-\infty}^{\infty} \frac{dx}{x} \tanh(\mu x) \frac{\sinh(\pi - \mu)x}{\sinh(\pi x)}, \quad (37)$$

where $\cos \mu = \sqrt{Q}/2$.

Having subtracted f_0 from $f_{ab}(L)$ we extrapolated the surface contributions and then the Casimir amplitudes using the BST algorithm. The results obtained for the Casimir amplitudes for different b.c. are presented in Table IV together with the conformal results. As for the critical exponents the results for the Ising model ($Q = 2$) are the most accurate, but good agreement between DMRG data and conformal results is found also for $Q = 3$. We stress that the numerical values for the

amplitudes are obtained from two successive BST extrapolations. In the case $Q = 4$ also the Casimir amplitudes are affected by logarithmic corrections. From the analysis of the extrapolants for the conformal anomaly, which can be obtained numerically from Eq. (36), we found that such quantity has logarithmic corrections of type $1/(\ln L)^2$. There are no theoretical predictions available about the form of these corrections. In the case of periodic b.c. it is instead known³⁸, from conformal results, that c has corrections of the type $1/(\ln L)^3$.

V. DISCUSSION

In this paper we have used the DMRG method to study the critical properties of the two dimensional Q state Potts model. Our study has demonstrated once again that, contrary to the widespread believe, the DMRG technique is able to describe accurately the critical region of a two dimensional classical (and consequently also of a one dimensional quantum) system. Indeed the numerical accuracy of the critical exponents calculated by our approach is comparable or even better than those of the other available numerical methods.

As was noticed in early studies the DMRG technique faces into problems to describe the critical region, in the thermodynamic limit of the infinite system method. In this case, as was shown by Östlund and Rommer⁷, the DMRG ground state is of a tensor product type, which can not describe algebraically decaying correlation functions, i.e. critical states. In the approach we used we have escaped this problem, since first, we applied the *finite system algorithm* and we restricted ourselves to lattices of moderate width, and second, we applied *symmetry breaking boundary conditions*. In the finite systems studied the correlation length remains always finite (and the transfer matrix spectrum is gapped), and the advantage of the boundary conditions is that one can calculate critical exponents from the non-vanishing value of the magnetization and energy density profiles. In the case of fixed-free boundary conditions from the same profile one can derive surface and bulk exponents.

To analyze the critical point data we borrowed the method of the traditional finite size scaling and used efficient sequence extrapolation techniques, such as the BST method. As known from the theory of asymptotic series analysis, one can obtain accurate limiting value by the method if i) the terms of the series are numerically very accurate and ii) there are no strong confluent singularities present. To satisfy the first requirement one needs a numerical accuracy of the data of at least $10^{-6} - 10^{-7}$, which can be achieved by the DMRG method, even at the critical point, if moderately large finite systems are studied. These systems, as demonstrated by our present study, are still about one order of magnitude larger than those diagonalized by the Lánczos algorithm and used in the traditional finite size scaling analysis.

In many physical problems the second requirement, i.e. the absence of (strong) confluent singularities is not satisfied and these corrections to scaling contributions represent the real limitations of the finite size scaling method. Since the strength of the confluent singularities decreases with the size of the systems one expects in many cases, like to our example with the $Q = 3$ and $Q = 4$ Potts models, more accurate results about the critical exponents by the DMRG analysis compared with the traditional finite size scaling.

In this paper we demonstrated another advantage of the DMRG method, namely at present it seems to be the only numerical method which could be used to study the density profiles in critical systems, especially in the parallel plate geometry¹¹. Our numerical studies on the profiles, together with the evaluation of the critical exponents in Sec. IV, have given strong numerical evidence that the conformal predictions about the critical density profiles of the Q state Potts model are exact in the scaling limit. Our results are satisfactory, even for the $Q = 4$ state model, in which case the first order finite size logarithmic corrections were taken consistently into account.

We mention that the analysis of this paper can be used and extended for other problems as well. For quantum Hamiltonians one expects similar or even better numerical accuracies, since the Hamiltonian is usually represented by a more sparse matrix than the transfer matrix of the equivalent classical problem. By this method one can also study such systems in which the critical point is not known exactly by duality. Finally one could also study first order phase transitions by the present approach, the results of this type of investigations will be presented elsewhere³⁹.

Acknowledgements - F.I.'s work has been supported by the Hungarian National Research Fund under grants No OTKA TO12830, OTKA TO23642 and OTKA TO17485 and by the Ministry of Education under grant No FKFP 0765/1997. He is indebted to the National Committee for Technological Development for a traveling grant (COST P1) and to the Institute for Theoretical Physics, Katholieke Universiteit Leuven, where part of this work has been completed, for kind hospitality. E.C. is financially supported by KULeuven Research Fund F/96/20. Useful discussions with A. Drzewiński, Ö. Legeza, I. Peschel, J. Sólyom and L. Turban are gratefully acknowledged.

¹ S. R. White, Phys. Rev. Lett. **69**, 2863 (1992).

² S. R. White and D. A. Huse, Phys. Rev. B **48**, 3844 (1993); E. S. Sørensen and I. Affleck, Phys. Rev. Lett. **71**, 1633 (1993); R. Bursill, T. Xiang and G. Gehring, J. Phys. A **28**, 2109 (1995).

³ S. R. White, R. M. Noack and D. J. Scalapino, Phys.

Rev. Lett. **73**, 886 (1994); M. Azzouz, L. Chen and S. Moukouri, Phys. Rev. B **50**, 6233 (1994); T. Narushima, T. Nakanura and S. Takada, J. Phys. Soc. Jpn. **64**, 4322 (1995); K. Hida, J. Phys. Soc. Jpn. **64**, 4896 (1995); U. Schollwöck and D. Ko, Phys. Rev. B **53**, 240 (1996).

⁴ R. M. Noack, S. R. White and D. J. Scalapino, Phys. Rev. Lett. **73**, 882 (1994).

⁵ S. R. White, Phys. Rev. Lett. **77**, 3633 (1996); S. R. White and D. J. Scalapino, Phys. Rev. B **55**, 6504 (1997); M. S. L. du Croo de Jongh and J. M. J. van Leeuwen, cond-mat/9709103.

⁶ M. Kaulke and I. Peschel (unpublished).

⁷ S. Östlund and S. Rommer, Phys. Rev. Lett. **75**, 3537 (1995).

⁸ I. Affleck, T. Kennedy, E. Lieb and H. Takashi, Phys. Rev. Lett. **59**, 799 (1987); Ö. Legeza, G. Fáth and J. Sólyom, Phys. Rev. B **55**, 291 (1997).

⁹ A. Drzewiński and J. M. J. van Leeuwen, Phys. Rev. B **49**, 403 (1994); A. Drzewiński and R. Dekeyser, Phys. Rev. B **51**, 15 218 (1995).

¹⁰ T. Nishino, J. Phys. Soc. Jpn. **64**, 3598 (1995).

¹¹ E. Carlon and A. Drzewiński, Phys. Rev. Lett. **79**, 1591 (1997).

¹² Y. Honda and T. Horiguchi, Phys. Rev. E to appear (Oct. 1997).

¹³ R. J. Baxter, *Exactly Solved Models in Statistical Mechanics* (Academic, London, 1982).

¹⁴ T. Nishino and K. Okunishi, J. Phys. Soc. Jpn. **65**, 891 (1995); preprint cond-mat/9705072

¹⁵ M. Barber in *Phase Transitions and Critical Phenomena* edited by C. Domb and J. L. Lebowitz (Academic, New York, 1983), vol. 8.

¹⁶ S. R. White, Phys. Rev. B **48**, 10 345 (1993).

¹⁷ For a review on the Potts model see: F. Y. Wu, Rev. Mod. Phys. **54**, 235 (1982).

¹⁸ R.J. Baxter, J. Phys. **C6**, L445 (1973).

¹⁹ Vl. S. Dotsenko, Nucl. Phys. **B235**, 671 (1984).

²⁰ J. L. Cardy in *Phase Transitions and Critical Phenomena* edited by C. Domb and J. L. Lebowitz (Academic, New York, 1987), vol. 11.

²¹ J. L. Cardy, Nucl. Phys. B **240**, 514 (1984).

²² M. den Nijs, J. Phys. **A12**, 1857 (1979); B. Nienhuis, E. K. Riedel and M. Schick, J. Phys. **A13**, L189 (1980); R. B. Pearson, Phys. Rev. B **22**, 2579 (1980).

²³ M. E. Fisher and P. G. de Gennes, C. R. Acad. Sci. Paris B **287**, 207 (1978).

²⁴ J. L. Cardy, Phys. Rev. Lett. **65**, 1443 (1990).

²⁵ T.W. Burkhardt and T. Xue, Phys. Rev. Lett. **66**, 895 (1991); Nucl. Phys. **B354**, 653 (1991).

²⁶ F. Iglói and H. Rieger, Phys. Rev. Lett. **78**, 2473 (1997).

²⁷ T. W. Burkhardt and E. Eisenriegler, J. Phys. **A18**, L83 (1985).

²⁸ K. Binder in *Phase Transitions and Critical Phenomena* edited by C. Domb and J. L. Lebowitz (Academic, New York, 1983), vol. 8.

²⁹ T. W. Burkhardt and J. L. Cardy, J. Phys. **A20**, L233 (1987).

³⁰ J. L. Cardy, M. Nauenberg and D. J. Scalapino, Phys. Rev. B **22**, 2560 (1980).

³¹ R. Bulirsch and J. Stoer, Num. Math. **6** 413 (1964); for applications in finite size scaling see c.f.: M. Henkel and G. Schütz, J. Phys. A **21**, 2617 (1988).

³² H. W. J. Blöte and P. Nightingale, Physica **112 A**, 405 (1982).

³³ J. Salas and A. D. Sokal, preprint hep-lat/9605018.

³⁴ F. Iglói, J. Phys. **A19**, 3077 (1986).

³⁵ D. Karevski, P. Lajkó and L. Turban, J. Stat. Phys. **86**, 1153 (1997).

³⁶ C. Vanderzande and A. L. Stella, J. Phys. A. **20** 3001, (1987).

³⁷ H. W. J. Blöte, A. Compagner, P. A. M. Cornelissen, A. Hoogland, F. Mallezie and C. Vanderzande, Physica **139 A**, 395 (1986).

³⁸ J. L. Cardy, J. Phys. **A19**, L1093 (1986).

³⁹ E. Carlon and F. Iglói (unpublished).